AGU PUBLICATIONS

JGR

Journal of Geophysical Research: Oceans

RESEARCH ARTICLE

10.1002/2015JC011455

Revisiting nitrification in the Eastern Tropical South Pacific: A focus on controls

Xuefeng Peng[1,2], Clara A. Fuchsman[3], Amal Jayakumar[1], Mark J. Warner[3], Allan H. Devol[3], and Bess B. Ward[1]

[1]Department of Geosciences, Princeton University, Princeton, New Jersey, USA, [2]Now at Department of Earth Science, Department of Chemical Engineering, University of California, Santa Barbara, CA, [3]School of Oceanography, University of Washington, Seattle, Washington, USA

Key Points:
- *In situ* NH_4^+, NO_2^-, and oxygen concentration and light control rates of NH_4^+ and NO_2^- oxidation
- NH_4^+ oxidation displayed extremely high affinity for both NH_4^+ and oxygen
- Ammonia oxidizers respond to *in situ* NH_4^+ concentrations/supply by adjusting their population size

Supporting Information:
- Supporting Information S1

Correspondence to:
X. Peng,
xpeng@princeton.edu

Citation:
Peng, X., C. A. Fuchsman, A. Jayakumar, M. J. Warner, A. H. Devol, and B. B. Ward (2016), Revisiting nitrification in the Eastern Tropical South Pacific: A focus on controls, *J. Geophys. Res. Oceans*, *121*, 1667–1684, doi:10.1002/2015JC011455.

Received 10 NOV 2015
Accepted 11 FEB 2016
Accepted article online 15 FEB 2016
Published online 12 MAR 2016

Abstract Nitrification, the oxidation of ammonium (NH_4^+) to nitrite (NO_2^-) and to nitrate (NO_3^-), is a component of the nitrogen (N) cycle internal to the fixed N pool. In oxygen minimum zones (OMZs), which are hotspots for oceanic fixed N loss, nitrification plays a key role because it directly supplies substrates for denitrification and anaerobic ammonia oxidation (anammox), and may compete for substrates with these same processes. However, the control of oxygen and substrate concentrations on nitrification are not well understood. We performed onboard incubations with ^{15}N-labeled substrates to measure rates of NH_4^+ and NO_2^- oxidation in the eastern tropical South Pacific (ETSP). The spatial and depth distributions of NH_4^+ and NO_2^- oxidation rates were primarily controlled by NH_4^+ and NO_2^- availability, oxygen concentration, and light. In the euphotic zone, nitrification was partially photoinhibited. In the anoxic layer, NH_4^+ oxidation was negligible or below detection, but high rates of NO_2^- oxidation were observed. NH_4^+ oxidation displayed extremely high affinity for both NH_4^+ and oxygen. The positive linear correlations between NH_4^+ oxidation rates and in situ NH_4^+ concentrations and ammonia monooxygenase subunit A (*amoA*) gene abundances in the upper oxycline indicate that the natural assemblage of ammonia oxidizers responds to *in situ* NH_4^+ concentrations or supply by adjusting their population size, which determines the NH_4^+ oxidation potential. The depth distribution of archaeal and bacterial *amoA* gene abundances and N_2O concentration, along with independently reported simultaneous direct N_2O production rate measurements, suggests that AOA were predominantly responsible for NH_4^+ oxidation, which was a major source of N_2O production at oxygen concentrations > 5 μM.

1. Introduction

Many facets of the nitrogen (N) cycling in the oceanic oxygen minimum zones (OMZs, oxygen concentrations $< \sim 5$ μM), have been studied during the past three decades. One of the primary motivations to understand N cycling in OMZs is that these regions account for a significant portion of fixed N removal from the ocean (25–58%) [*DeVries et al.*, 2012] despite their small volume (~0.1% of total ocean volume) [*Codispoti et al.*, 2001]. While tremendous progress has been made in understanding N cycling processes, incomplete knowledge of controls on each specific process has fueled ongoing studies on OMZs. Nitrification is one of the key N cycling processes that is still not well understood in OMZs.

Nitrification consists of two sequential steps: the oxidation of ammonium (NH_4^+) to nitrite (NO_2^-) and then to nitrate (NO_3^-). Nitrification could directly supply substrates for denitrification and anaerobic NH_4^+ oxidation (anammox), or compete for substrates with the same processes. In the eastern tropical South Pacific (ETSP), NH_4^+ oxidation was suggested to account for 6–33% of the total NO_2^- production in the upper OMZ [*Lam et al.*, 2009]. A following study in the same region showed that NH_4^+ oxidation supplied only ~7% of the total NO_2^- production [*Kalvelage et al.*, 2013]. These data highlight the uncertainty about the contribution of NH_4^+ oxidation to NO_2^- supply for denitrification and anammox.

NH_4^+ oxidation is mediated by ammonia-oxidizing archaea (AOA) and bacteria (AOB); NO_2^- oxidation is mediated by nitrite-oxidizing bacteria (NOB). These groups are all obligate aerobes but are apparently microaerophilic and function well at very low oxygen concentrations. Natural assemblages of ammonia oxidizers [*Horak et al.*, 2013; *Newell et al.*, 2013] and pure cultures of marine AOA [*Martens-Habbena et al.*, 2009]

have demonstrated high affinity for NH_4^+. The ubiquitous AOA are considered predominantly responsible for NH_4^+ oxidation in the ocean [*Beman et al*., 2012; *Newell et al*., 2013; *Santoro et al*., 2010].

The ultimate source of NH_4^+ for nitrification in the water column is remineralization of organic matter produced in the euphotic zone, which exerts a first-order control on nitrification rates [*Kalvelage et al*., 2013; *Newell et al*., 2011; *Ward and Zafiriou*, 1988]. OMZs are characterized by their high productivity in the euphotic zone, which in turn fuels remineralization, creating a sharp oxycline reaching oxygen levels below detection. A poorly ventilated anoxic layer underlies the upper oxycline. The strong vertical oxygen gradient in OMZs should be another key control of aerobic NH_4^+ oxidation, for which molecular oxygen is required. The physiological control by oxygen on NH_4^+ oxidation has been studied both in culture and in the environment. The cultivated AOA *N. maritimus* demonstrated a low half-saturation concentration for oxygen (K_m = 3.9 μM) [*Martens-Habbena et al*., 2009], and a natural assemblage collected from the ETSP displayed an even higher affinity for oxygen (K_m = 330 nM) [*Bristow et al*., 2013]. Such high affinity for oxygen by ammonia oxidizers suggests that NH_4^+ oxidation rates are only sensitive to oxygen concentrations at very low levels.

The subunit A of the ammonia monooxygenase enzyme (encoded by the gene *amoA*), which functions to insert an oxygen atom into ammonia during the first step of NH_4^+ oxidation, is found in both AOA and AOB. The archaeal and bacterial *amoA* genes are commonly used as a molecular marker to enumerate AOA and AOB in the environment. While a few previous studies in marine water columns have found a positive correlation between the abundance of AOA and NH_4^+ oxidation rates [*Beman et al*., 2008; *Smith et al*., 2014a], the correlation was not ubiquitous. For example, $> 10^3$ copies of archaeal *amoA* gene per mL seawater have been reported at anoxic depths of the major OMZs, where NH_4^+ oxidation rates were undetectable or negligible [*Lam et al*., 2009; *Newell et al*., 2011]. We measured the archaeal and bacterial *amoA* gene abundances at two stations at relatively high depth resolution in order to resolve the relationship between rates and abundances in both oxic and anoxic zones.

Like NH_4^+ oxidation, the distribution of NO_2^- oxidation in OMZs should also be controlled by oxygen concentrations. A Michaelis-Menten relationship between NO_2^- oxidation rates and oxygen concentration in both the ETSP (K_m = 0.78 μM) [*Bristow et al*., 2013] and the Namibian OMZs (K_m = ~4 μM) [*Fussel et al*., 2012] was reported previously. Both studies determined NO_2^- oxidation rates using incubations with $^{15}NO_2^-$ and manipulated the oxygen level using additions of oxygen-saturated seawater. However, high rates of NO_2^- oxidation have been measured at the anoxic depths of OMZs, where no alternative electron acceptors are known [*Beman et al*., 2013; *Kalvelage et al*., 2013; *Lipschultz et al*., 1990; *Peng et al*., 2015]. No satisfactory explanations have been provided for this puzzle of how high NO_2^- oxidation rates can occur at essentially zero oxygen concentrations.

The main goal of this study was to determine the depth distribution of NH_4^+ and NO_2^- oxidation rates over chemical gradients in the ETSP OMZ. Additional experiments were performed to investigate the substrate dependence of NH_4^+ and NO_2^- oxidation and to examine the effects of metal additions and photoinhibition on nitrification. Nitrification as a source of NO_3^- in the euphotic zone is often ignored because nitrification is assumed to be inhibited by light. The photoinhibition of nitrification is not complete, however, indicating that both *in situ* nitrification and physical processes provide NO_3^- for uptake by phytoplankton [*Dore et al*., 1996; *Ward et al*., 1989]. Our data, along with nitrification rates measured in other OMZs, demonstrate that NH_4^+ and oxygen concentrations and light levels are critical controls of NH_4^+ and NO_2^- oxidation rates in the upper oxycline of OMZs.

2. Methods

2.1. Site Description and Physicochemical Data Collection

Nitrification incubations were performed at 8 stations in the ETSP in June and July 2013 on board the R/V Nathanial B. Palmer (Figure 1). Two of the stations (BB2 and 21) were coastal (<50 km offshore, bottom depth = 1625 and 2207 m, respectively), characterized by higher surface chlorophyll levels than the rest of the stations, which were offshore (> 200 km offshore, bottom depths >3500 m). Stations BB1 and BB2 were sampled with greater resolution than the other stations. Concentrations of NH_4^+, NO_2^-, and NO_3^- were determined by standard spectrophotometric methods onboard, with detection limits of 0.06 μM for NH_4^+, 0.03 μM for NO_2^-, and 0.10 μM for NO_3^- [*UNESCO*, 1994]. Dissolved oxygen concentration was determined

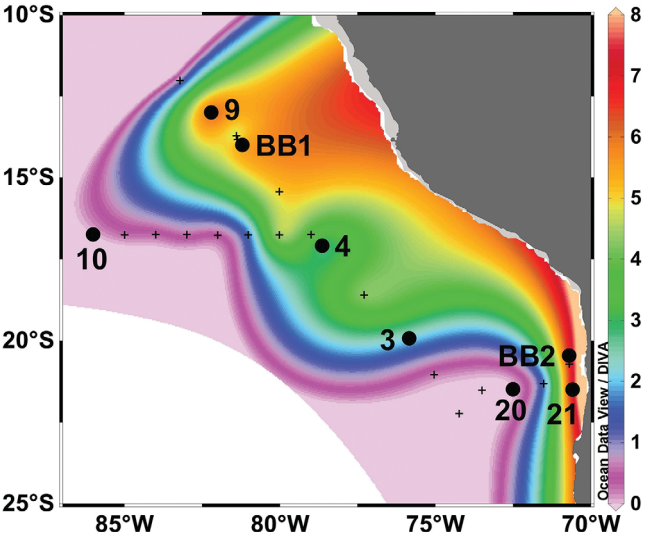

Figure 1. Locations of nitrification rate incubation experiments during the cruise in June and July 2013 to the eastern tropical South Pacific, onboard R/V Nathanial B. Palmer. Crosses represent additional stations during the cruise from which chemical data were collected. Contour lines show NO_2^- concentrations (μM) at 250 m depth.

using the SBE 43 dissolved oxygen sensor attached to a SBE 911+ Conductivity, Temperature and Depth (CTD) system. For some of the casts, a STOX sensor was also deployed with the CTD to measure oxygen concentration [*Revsbech et al.*, 2009]. The main objective of using the STOX sensor was to define the depth range and region of anoxia in the OMZ to aid in selecting sample depths, which is possible because the STOX sensor has an extremely low detection limit [*Revsbech et al.*, 2009]. Thus the STOX sensor, when available, was used to select the sample depths, but the values reported here are from the SBE 43 sensor, because it provided a complete coverage of all stations sampled on this cruise.

2.2. N_2O Measurements

Dissolved N_2O concentrations were measured using a modified version of the sampling and analytical methods developed for the measurements of the dissolved transient tracers - chlorofluorocarbons 11 and 12 and sulfur hexafluoride by *Bullister and Wisegarver* [2008]. Water samples were collected into 250 cm^3 ground glass syringes through a plastic three-way stopcock inserted directly into the Niskin bottle petcock. These samples were stored at 3–5°C until 30–45 min. before analysis. They were then heated to approximately 35°C prior to analysis.

Concentrations of N_2O were measured by shipboard electron capture gas chromatography (EC-GC). The gas was introduced to the EC-GC via a purge-and-trap technique developed by D. P. Wisegarver and J. L. Bullister (personal communication, 2013). Approximately 200 mL of water sample were purged with nitrogen and the compounds of interest were trapped on a Porapak Q/Carboxen 1000/Molecular Sieve 5A trap cooled by an immersion bath to −60°C. The major modifications to the analytical system described by *Bullister and Wisegarver* [2008] are the additions of a second precolumn (13 cm of 80/100 mesh molecular sieve 5A) to separate the N_2O from the CFCs and an analytical column for N_2O (30 cm of molecular sieve 5A) in a 220°C oven. Instrumental grade P-5 gas (95% Ar/5% CH_4) was directed onto the second precolumn and into the third column for the N_2O analyses.

The analytical system was calibrated frequently using a standard gas of known composition in gas sample loops of known volume at measured temperatures and pressures. The procedures used to transfer the standard gas to the trap, precolumns, main chromatographic columns and EC detectors were similar to those used for analyzing water samples. Full-range calibration curves were run at the beginning and end of the cruise, and they were supplemented with occasional injections of multiple aliquots of the standard gas at more frequent time intervals.

On this expedition, based on the analysis of 15 duplicate samples, we estimate precisions (1 standard deviation) as the larger of 1.9 nmol kg^{-1} or 3.5% for dissolved N_2O.

2.3. Onboard Incubation Experiments

Approximately 450 mL of seawater was transferred from Niskin (10 L) bottles into opaque, metal-free, gas-tight, tri-laminate bags avoiding contact with the atmosphere. The bottles from anoxic depths were sampled first as soon as the CTD system arrived on deck. Degassed ^{15}N tracer solutions (in a vacuum chamber for >30 min prior to the incubation to remove dissolved oxygen) were injected during the filling process to ensure complete mixing. $^{15}NH_4^+ + {}^{14}NO_2^-$ were added for NH_4^+ oxidation incubations, and $^{15}NO_2^-$ was added for NO_2^- oxidation incubations. The final concentration of ^{15}N substrates and the ^{14}N carrier reached ~ 400 nM (calculated using the ^{15}N substrates stock concentration and the final volume of the incubation), which should be above the substrate saturation concentration for nitrification [*Horak et al*., 2013; *Newell et al*., 2013; *Qin et al*., 2014]. The bags were incubated in an incubator or cold room at a temperature close to the *in situ* temperature (within 0 – 5.7°C of *in situ* temperature). After ~18 h of incubation, a 45 mL aliquot of the sample was transferred to a 50 mL centrifuge tube and stored at −80°C.

2.4. Measurement of NH_4^+ Oxidation

The stable isotope ratio of NO_2^- in the samples was measured following the azide method of *McIlvin and Altabet* [2005], which converts NO_2^- into N_2O. The details were described in *Peng et al*. [2015]. The concentration of N_2O and ratio of $^{45}N_2O/^{44}N_2O$ were determined on a Delta V Plus isotope ratio mass spectrometer coupled to a purge-and-trap front end. The detection limit was 0.2 nmol of N, and the precision of $\delta^{15}N$ was 0.2‰. ($\delta^{15}N = (R^{15}N_{sample}/R^{15}N_{reference} - 1) \times 1000‰$, where $R^{15}N$ is ratio of ^{15}N to ^{14}N molecules in the sample or reference material, and atmospheric N_2 is used as a reference here.)

The rate of NH_4^+ oxidation was calculated following the equation:

$$V_{NH_4^+} = \frac{\Delta[^{15}NO_2^-]}{f^{15}_{NH_4^+} \times T}$$

where $\Delta[^{15}NO_2^-]$ is the change in concentration of $^{15}NO_2^-$ between the start and the end of the incubation as a result of NH_4^+ oxidation, $f^{15}_{NH_4^+}$ is the fraction of NH_4^+ that was labeled with ^{15}N at the start of the incubation, and T is the length of incubation. The concentration of $^{15}NO_2^-$ at the start of the incubation ($[^{15}NO_2^-]_0$) was calculated from the measured ambient NO_2^- concentration assuming natural abundance $\delta^{15}N\text{-}NO_2^-$. The actual value of natural abundance $\delta^{15}N\text{-}NO_2^-$ for each sample was taken from a depth profile at the closest station in the ETSP reported by *Casciotti et al*. [2013]. For samples collected from depths shallower than the anoxic layer, the $[^{15}NO_2^-]_0$ was calculated with the natural abundance $\delta^{15}N\text{-}NO_2^-$ reported for the depth that had the same oxygen concentration as the published depth profile [*Casciotti et al*., 2013]. For samples collected from the anoxic depths, the $[^{15}NO_2^-]_0$ was calculated with the natural abundance $\delta^{15}N\text{-}NO_2^-$ reported for depths with the same NO_2^- concentration corresponding to their relationship to the secondary nitrite maximum (i.e., above or below the SNM) in the published depth profile [*Casciotti et al*., 2013]. For the two samples collected from 1000 m (deeper than the anoxic layer), the $[^{15}NO_2^-]_0$ was calculated assuming a $\delta^{15}N\text{-}NO_2^-$ of 0 ‰. Rates were not particularly sensitive to variability of initial $\delta^{15}N\text{-}NO_2^-$ in a reasonable range. Sensitivity tests demonstrated that fluctuations of the natural abundance $\delta^{15}N\text{-}NO_2^-$ by ±5 ‰ would result in negligible differences in calculated ammonia oxidation rates (supporting information Figure S1).

2.5. Measurement of NO_2^- Oxidation

The $\delta^{15}N\text{-}NO_3^-$ was measured using the denitrifier method [*McIlvin and Casciotti*, 2011; *Sigman et al*., 2001]. Samples were first treated with 15 mM sulfamic acid (final concentration) for 30 min to remove any preexisting NO_2^-, and the pH was raised to ~7 with NaOH [*Granger and Sigman*, 2009]. The efficiency of NO_2^- removal was > 97.5%, and the trace amount of contaminating $^{15}NO_3^-$ was accounted for as in *Peng et al*. [2015]. Three NO_3^- international reference materials (IAEA-N3, USGS 34, and USGS 32) were used to calibrate the $\delta^{15}N\text{-}NO_3^-$.

The rate of NO_2^- oxidation was calculated following the equation:

$$V_{NO_2^-} = \frac{\Delta[^{15}NO_3^-]}{f^{15}_{NO_2^-} \times T}.$$

where $\Delta[^{15}NO_3^-]$ is the change in concentration of $^{15}NO_3^-$ between the start and the end of the incubation as a result of NO_2^- oxidation, $f^{15}_{NO_2^-}$ is the fraction of NO_2^- that was labeled with ^{15}N at the start of the incubation, and T is the length of incubation. The $[^{15}NO_3^-]$ at the start of the incubation ($[^{15}NO_3^-]_0$) was calculated from the measured ambient NO_3^- concentration assuming natural abundance $\delta^{15}N\text{-}NO_3^-$. The actual value of natural abundance $\delta^{15}N\text{-}NO_3^-$ for each sample was taken from a depth profile at the closest station in the ETSP reported by *Casciotti et al.* [2013]. For samples collected from depths shallower than the anoxic layer, the $[^{15}NO_3^-]_0$ was calculated with the natural abundance $\delta^{15}N\text{-}NO_3^-$ reported for the depth that had the same oxygen concentration on the published depth profile [*Casciotti et al.*, 2013]. For samples collected from the anoxic depths, the $[^{15}NO_3^-]_0$ was calculated with the natural abundance $\delta^{15}N\text{-}NO_3^-$ reported for depths with the same NO_2^- concentration corresponding to their relationship to the SNM (i.e., above or below the SNM) in the published depth profile [*Casciotti et al.*, 2013]. For the two samples collected from 1100 m (deeper than the anoxic layer), the $[^{15}NO_3^-]_0$ was calculated assuming a $\delta^{15}N\text{-}NO_3^-$ of 5 ‰. We did not account for isotope dilution by regeneration of the ^{15}N-labeled N substrate, so the calculated NH_4^+ and NO_2^- oxidation rates calculated may be underestimations.

2.6. Detection Limit of Rate Measurements

The detection limit was determined for every individual incubation following *Santoro et al.* [2013], and depends on the fraction of the substrate labeled with ^{15}N at the beginning of the incubation as well as the concentration of the product pool. For samples from anoxic depths, the azide method (used for NH_4^+ oxidation measurements) had a detection limit of 0.01–0.10 nM d^{-1}, and the denitrifier method (used for NO_2^- oxidation measurements) of 0.20–4.26 nM d^{-1}. For the rest of the samples, the azide method had a detection limit of 0.003–0.065 nM d^{-1}, and the denitrifier method of 0.01–0.51 nM d^{-1}. The azide method had a higher sensitivity than the denitrifier method, mainly because the NO_2^- concentrations were lower than the NO_3^- concentrations. The samples from anoxic depths had relatively higher detection limits due to the presence of high NO_2^- concentrations, which results in a higher concentration product pool for the NH_4^+ oxidation measurements, and a lower substrate fraction labeled with ^{15}N for the NO_2^- oxidation measurements.

2.7. Kinetics Experiments

The dependence of NH_4^+ oxidation on NH_4^+ availability was tested by incubating seawater samples at five different levels of $^{15}NH_4^+$ addition (20, 50, 100, 200, and 500 nM), at both stations BB1 and BB2. Seawater was collected from 75 m at station BB1 and 30 m at station BB2, depths which were intended to target the primary nitrite maximum (PNM). However, NO_2^- concentration measurements showed that 75 m at station BB1 was slightly (by ~10 m) below the PNM, and 30 m at station BB2 was slightly (by ~10 m) above the PNM. The dependence of NO_2^- oxidation on NO_2^- availability was tested by incubating seawater samples at five different levels of $^{15}NO_2^-$ addition (20, 50, 100, 200, and 500 nM) at station BB2. Seawater was collected from 70 m to target the depth of a NO_2^- concentration minimum between the PNM and the secondary nitrite maximum (SNM).

2.8. Light/Dark Experiments on Nitrification

At stations BB1 and BB2, an additional experiment was performed to investigate photoinhibition of NH_4^+ and NO_2^- oxidation. Seawater from 20 m was sampled in the early morning and the incubations were performed in 150 mL clear polycarbonate bottles, which were placed in a seawater incubator installed on deck with mesh screen to reduce the light to ~10% of surface irradiance. A parallel set of samples was incubated in the dark in a seawater incubator. The light level in the incubators was measured throughout the day using an underwater spherical quantum sensor (LI-COR, Lincoln, NE). The incubation was terminated just before sunset.

2.9. Quantification of Archaeal and Bacterial amoA Genes

At the process stations (BB1 and BB2) particulate material was collected by filtering 2.5 - 10 liters of seawater through 0.22 μm Sterivex filters with a peristaltic pump. Nucleic acids were extracted as described previously [*Peng et al.*, 2013]. Archaeal and β-proteobacterial *amoA* gene copies were enumerated using qPCR in triplicate as described previously, using the QuantiTect SYBR Green PCR Kit [*Newell et al.*, 2011].

Primers Arch-amoAF (5′-STAATGGTCTGGCTTAGACG-3′) and Arch-amoAR (5′-GCGGCCATCCATCTGTATGT-3′) [*Francis et al.*, 2005] were used for archaeal *amoA* gene quantification, and primers amoA-1F (5′-GGGGTTTCTACTGGTGGT-3′) and amoA-2R (5′-CCCCTCKGSAAAGCCTTCTTC-3′) [*Rotthauwe et al.*, 1997] for β-proteobacterial *amoA* gene quantification. The detection limit for both archaeal and β-proteobacterial *amoA* gene qPCR assays was approximately 100 copies per assay. Therefore the sensitivity depends on the amount of DNA extracted from different volumes at different depths, and would translate to approximately 5–10 gene copies per mL of seawater.

2.10. Alternative Electron Acceptor Experiment

Additional experiments were performed to test the response of NH_4^+ oxidation at anoxic depths to the addition of oxygen and alternative electron acceptors (iron and manganese). At stations 9 and BB2, seawater from the deep chlorophyll maximum (DCM) and the SNM was collected to fill 12 mL exetainers (overflowing the exetainers by 3 volumes), which were sealed immediately to minimize oxygen contamination. Exetainers were covered in aluminum foil to reduce exposure to light. $^{15}NH_4^+ + {}^{14}NO_2^-$ (final concentration 600 nM) was added to four groups of parallel incubations. The first group served as a control without anything else added; the second group was supplemented with 0.5 mL of oxygen-saturated seawater to reach a final oxygen concentration of 9.6 μM; the third group was supplemented with Fe_2O_3 (final concentration 6.1 nM); and the fourth group was supplemented with MnO_2 (final concentration 12.7 nM). Immediately after adding the ^{15}N substrate and Fe_2O_3/MnO_2, the exetainers were purged with Ultra High Purity Helium for 5 min to remove any oxygen that could have been introduced. The incubations supplemented with oxygen were purged before adding the oxygen-saturated seawater. The incubations were performed in the dark for 24 h. At the end of the incubation, the entire incubation volume was transferred to a 15 mL centrifuge tube and stored at −80°C.

3. Results

3.1. Chemical Characteristics of the ETSP OMZ

The degree of anoxia and the distribution of associated chemical concentrations in the water column varied widely among stations, which could be divided into three regimes: coastal OMZs, offshore OMZs, and OMZ margins. Coastal OMZs include stations BB2 and 21 (Figure 1), which are characterized by a thick anoxic layer (> 300 m) and high NO_2^- accumulation (up to 8 μM) in the anoxic layer (Figures 2a and 2b). N_2O concentration at coastal OMZs showed two peaks, which were located in the upper and lower oxyclines near the oxic-anoxic interfaces (Figure 2d). The N_2O concentration peak in the upper oxycline covered a smaller depth range (< 50 m) than the one in the lower oxycline (> 600 m). NH_4^+ concentration at coastal OMZs decreased rapidly with depth, and a subsurface maximum (> 1.5 μM) was detected at station BB2 (Figure 2a).

Offshore OMZs include stations BB1, 3, and 4 (Figure 1), which are also defined by an anoxic layer (< 300 m thick), but the SNM was thinner compared to coastal OMZs (Figures 3a and 3b). The depth profile of N_2O concentration at station BB1 was similar to that at coastal OMZs (Figure 3d; N_2O concentration was not measured at all stations). NH_4^+ concentration at offshore OMZ stations decreased rapidly with depth (from > 0.4 μM to below detection), except at station 3 where the NH_4^+ concentration near the surface was not higher than at depth (Figure 3a).

OMZ margins include stations 10 and 20, where no obvious SNM was detected, the anoxic layer was thinner (Figures 4a and 4b) and a distinct primary NO_2^- maximum was present. At station 20, there was a subsurface maximum of N_2O concentration in the upper oxycline, but no measurements were made to define the depth profile below 200 m (Figure 4d). N_2O concentration at station 10 increased with depth but no subsurface maximum in the upper water column was detected. NH_4^+ concentration decreased rapidly with depth, and a subsurface maximum was evident at station 10 (Figure 4a).

3.2. NH_4^+ Oxidation Rates

NH_4^+ oxidation rates were low or undetectable in the surface waters, but reached a subsurface maximum in the upper oxycline at all stations. The maximum rate of NH_4^+ oxidation at coastal OMZs was higher than that at the offshore OMZs and OMZ margins. At coastal station BB2, we captured a single maximum NH_4^+ oxidation rate of 77 nM d^{-1} (Figure 2c). At most of the other stations, NH_4^+ oxidation rates reached a

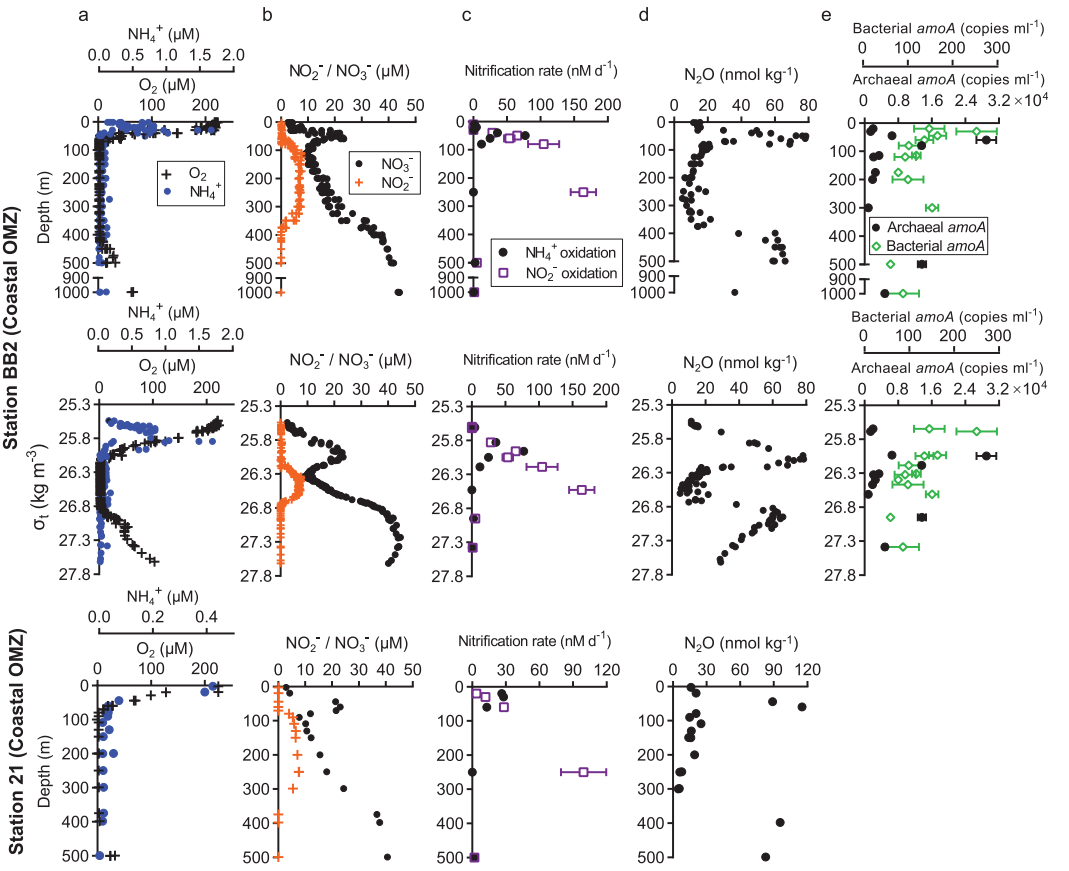

Figure 2. Rates, chemical, and *amoA* gene abundance profiles at the coastal OMZ stations BB2 and 21. (a) Oxygen and NH_4^+ concentration (μM); (b) NO_2^- and NO_3^- concentration (μM); (c) NH_4^+ and NO_2^- oxidation rates; (d) N_2O concentration (nmol kg^{-1}); (e) archaeal and β-proteobacterial *amoA* gene abundance quantified with qPCR. The middle plot shows the profiles at station BB2 against density anomaly, σ_t (kg m^{-3}), which extended to 1674 m. No *amoA* gene abundance was measured at station 21. Error bars in Figure 2c represent the standard deviation of two replicates, and error bars in Figure 2e represent the standard deviation of three replicates. Where the error bars are not visible, they are smaller than the data markers.

maximum between 25 and 35 nM d^{-1}. Relatively low NH_4^+ oxidation rates (< 8 nM d^{-1}) were measured at stations 3 (offshore OMZ, Figure 3c) and 10 (OMZ margin, Figure 4c). At all stations with N_2O concentration measurements except station 10 (OMZ margin), the depth of the subsurface maximum of NH_4^+ oxidation rate was very similar to that of the maximum N_2O concentration in the upper oxycline. NH_4^+ oxidation rates were either below detection or negligible (0.35–0.44 nM d^{-1}) in the anoxic layer and detectable but very low in the lower oxycline (0.44–2.68 nM d^{-1}) at all stations.

NH_4^+ oxidation rates under 10% surface irradiance (up to 170 μE m^{-2} s^{-1}, see supporting information Figure S2) were partially inhibited to a level about a third of the uninhibited rates in the dark (Table 1). In contrast, NO_2^- oxidation rates were not significantly different between the two light conditions.

The addition of oxygen, Fe_2O_3, and MnO_2 to samples collected at the SNM and the DCM did not increase NH_4^+ oxidation rates significantly (t-test $p > 0.05$) over rates detected in the control experiments, except at the deep chlorophyll maximum at station BB2 (65 m). In this sample, the addition of 9.6 μM of oxygen stimulated the NH_4^+ oxidation rate by eight-fold (Figure 5). The addition of 6.1 nM Fe_2O_3 also increased the NH_4^+ oxidation rate in one but not the other of the two replicate incubations, so the result was not statistically significant (t-test $p > 0.05$).

3.3. NO_2^- Oxidation Rates

High rates of NO_2^- oxidation (up to ~100 nM d^{-1}) were found at the oxic-anoxic interface in the upper oxycline and in the anoxic layer at all stations (Figures 2c–4c). NO_2^- oxidation rates were generally much higher

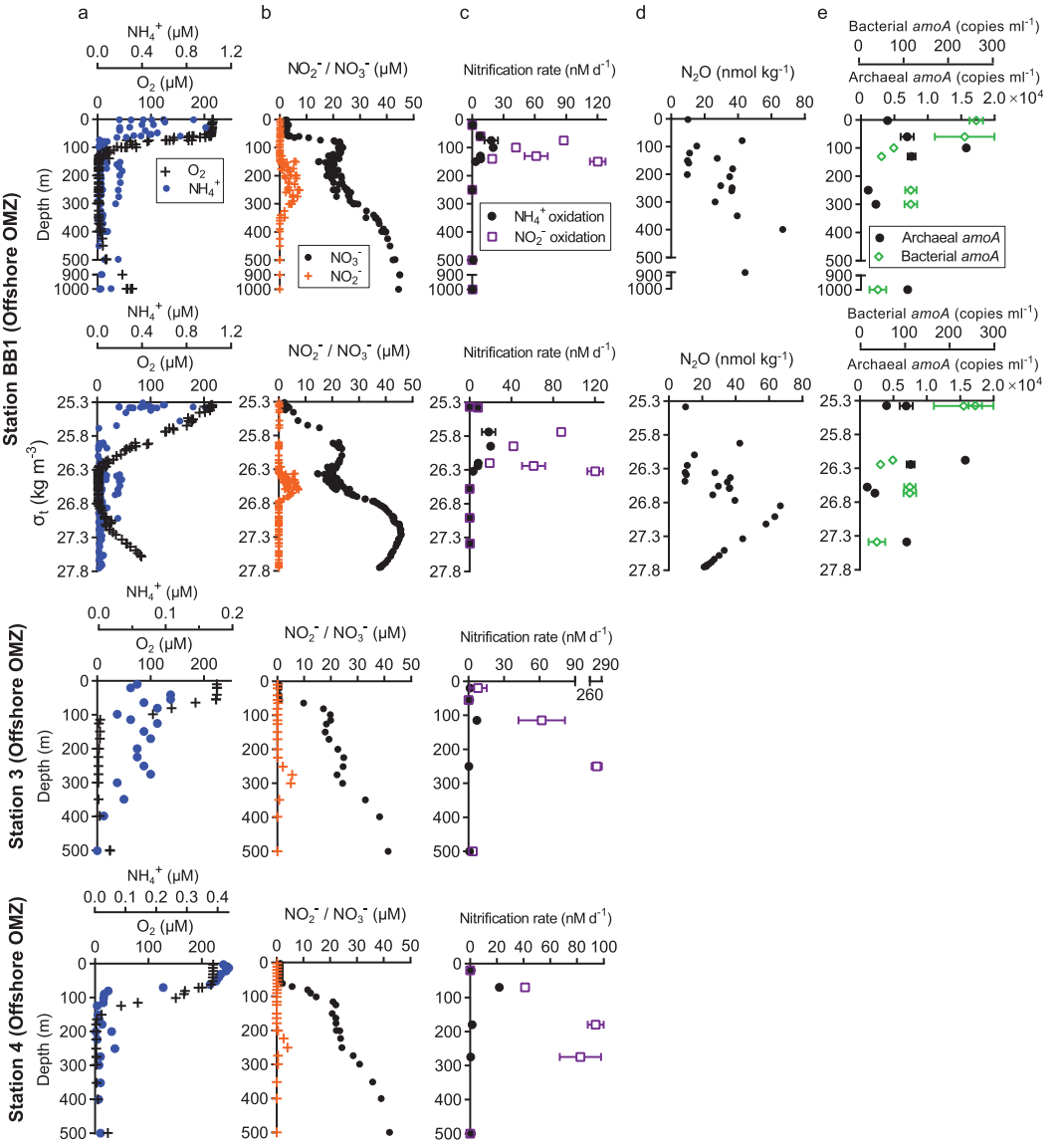

Figure 3. Rates, chemical, and *amoA* gene abundance profiles at the offshore OMZ stations BB1, 3, and 4. Plots and symbols are the same as in Figure 2. The deepest depth in the profile against σ_t is 3500 m. N_2O concentration and *amoA* gene abundance were not measured at stations 3 and 4.

than NH_4^+ oxidation rates, especially in the anoxic layer, where NH_4^+ oxidation rates were negligible but NO_2^- oxidation rates were high. NO_2^- oxidation rates were never detected in the shallowest samples (within the euphotic zone above the oxycline) at each station. At depths greater than 400 m, no NO_2^- oxidation was detected except at station 20, at the low rate of 6.2 nM d^{-1}. At station 10 (OMZ margin), NO_2^- oxidation rates were low or undetectable overall, except at the oxic-anoxic interface, where there is a small amount of NO_2^- accumulation (0.04 μM).

3.4. Abundance of amoA Genes

The depth profile of archaeal *amoA* gene abundances at stations BB1 and BB2 resembled that of NH_4^+ oxidation rates, in that both showed subsurface maxima in the upper oxycline (Figures 2e and 3e). The archaeal *amoA* gene abundances at the shallowest depths (2.5 – 30 m) were a few thousand copies mL^{-1}. The subsurface maximum of archaeal *amoA* gene abundance (1.6×10^4 copies mL^{-1} at offshore station BB1 and 2.9×10^4 copies mL^{-1} at coastal station BB2) coincided with the subsurface maximum of N_2O

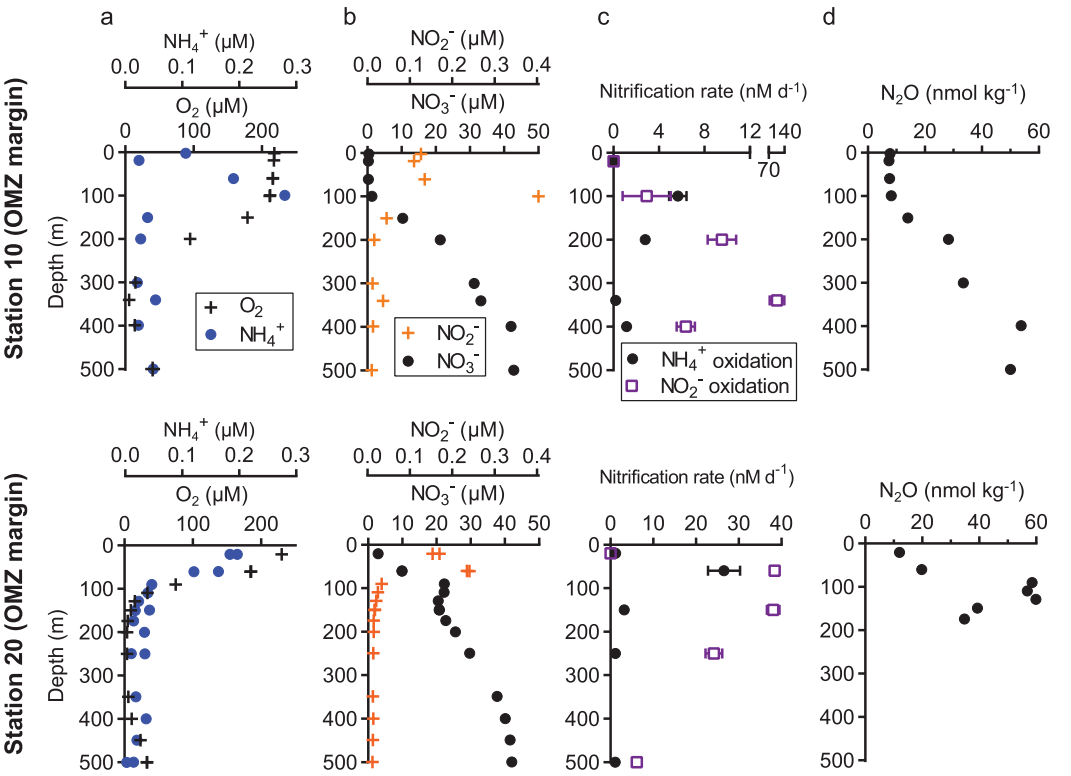

Figure 4. Rates and chemical profiles at OMZ margin stations 10 and 20. Plots and symbols are the same as in Figure 2. No *amoA* gene abundance was measured at these stations.

concentration. Substantial numbers of archaeal *amoA* genes (thousands of copies mL^{-1}) were enumerated at the anoxic depths and the lower oxycline, where NH_4^+ oxidation rates were either negligible or very low.

The abundance of β-proteobacterial *amoA* genes was overall 1 - 2 orders of magnitude lower than that of archaeal *amoA* genes (Figures 2e and 3e). The maximum β-proteobacterial *amoA* gene abundance (~250 copies mL^{-1}) was found in the surface layer at both stations BB1 and BB2. Unlike the archaeal *amoA* gene abundance, β-proteobacterial *amoA* gene abundance remained low at all depths below the subsurface maximum.

3.5. Nitrification Kinetics

NH_4^+ oxidation rates displayed a classic Michaelis-Menten dependence on NH_4^+ concentration in the kinetics experiment at the PNM at station BB1, with a half-saturation concentration of 27.4 ± 4.4 nM (Figure 6). The maximum NH_4^+ oxidation rate of this water sample (24.9 ± 1.3 nM d^{-1}) was reached around 125 nM NH_4^+. By contrast, no apparent response was observed to the different levels of ^{15}N substrate addition at station BB2 (supporting information Figure S3), probably due to the high ambient concentrations of NH_4^+ (1.48 μM at 30 m) and NO_2^- (2.79 μM at 70 m).

Grouping all measurements by their vertical position in the ETSP revealed different relationships or lack thereof between NH_4^+ oxidation rates and NH_4^+ concentrations (Figure 7a). There was a robust positive linear correlation between NH_4^+ oxidation rates and NH_4^+ concentrations in the upper oxycline ($R^2 = 0.82$, $p < 0.0001$). No clear relationships between NH_4^+ oxidation rates and NH_4^+ concentrations were observed in the euphotic zone. In the anoxic layer and depths below it, NH_4^+ concentration was very low and was above detection limit (0.06 μM) in

Table 1. A Comparison of NH_4^+ and NO_2^- Oxidation Rates (Average ± 1 Standard Deviation, n = 3) Measured at 10% Surface Irradiance and in the Dark[a]

Station	Light/Dark	NH_4^+ Oxidation Rate (nM d^{-1})	NO_2^- Oxidation Rate (nM d^{-1})
BB1	10% Light	0.94 ± 0.07	12.52 ± 1.71
	Dark	3.27 ± 0.19	8.85 ± 6.64
BB2	10% Light	0.35 ± 0.01	4.68 ± 4.35
	Dark	1.00 ± 0.02	0.00 ± 0.00

[a]Samples were taken from 20 m in the early morning at stations BB1 (offshore) and BB2 (coastal).

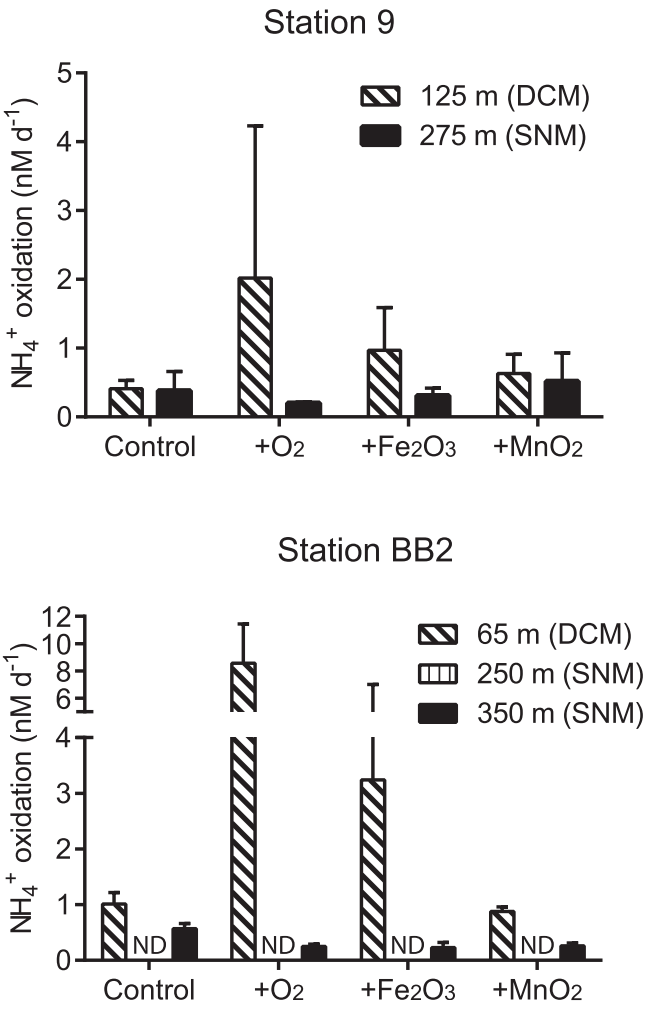

Figure 5. NH_4^+ oxidation rates measured at the deep chlorophyll maximum (DCM) and secondary nitrite maximum (SNM) at stations 9 and BB2. These incubations were done with He-flushed seawater in gas-tight vials. All incubations received 600 nM of $^{15}NH_4^+$ (final concentration). Except for the Control, one of the three electron acceptors was also added to the incubation (9.6 μM of O_2, 6.1 nM of Fe_2O_3, and 12.7 nM of MnO_2). No rates were detected (ND) at 250 m at station BB2. Error bars represent standard deviations of 2 replicates.

only two samples (250 m at station 3 and 1000 m at station BB2). In the upper oxycline, NO_2^- oxidation rates appeared to be positively related to NO_2^- concentration (Figure 7b). In particular, at NO_2^- concentrations < 0.1 μM, there was a positive linear correlation between NO_2^- oxidation rates and NO_2^- concentration ($R^2 = 0.68$, $p < 0.01$).

When results from all stations were combined, NH_4^+ oxidation rates in the upper oxycline showed a Michaelis-Menten-like relationship ($p < 0.05$) with oxygen concentration (Figure 8a). In contrast, NO_2^- oxidation rates displayed a nonlinear inverse relationship with oxygen concentration (Figure 8b). For the six samples in which both NH_4^+ oxidation rates and *amoA* gene abundance were measured, per cell NH_4^+ oxidation rates were calculated assuming each ammonia oxidizer carries one copy of either archaeal or bacterial *amoA* gene (Figure 9). The per cell NH_4^+ oxidation rates demonstrated a Michaelis-Menten relationship with *in situ* oxygen concentrations ($p < 0.01$), with a half-saturation concentration of 2.0 ± 1.2 μM and a maximum per cell NH_4^+ oxidation rate of 1.14 ± 0.15 fmol $cell^{-1}$ d^{-1}.

4. Discussion

4.1. Key Chemical Features of the ETSP OMZ

The degree of anoxia and NO_2^- accumulation in the anoxic layer in the region likely reflects the amount of organic matter input from the surface layer, because organic matter remineralization in the water column

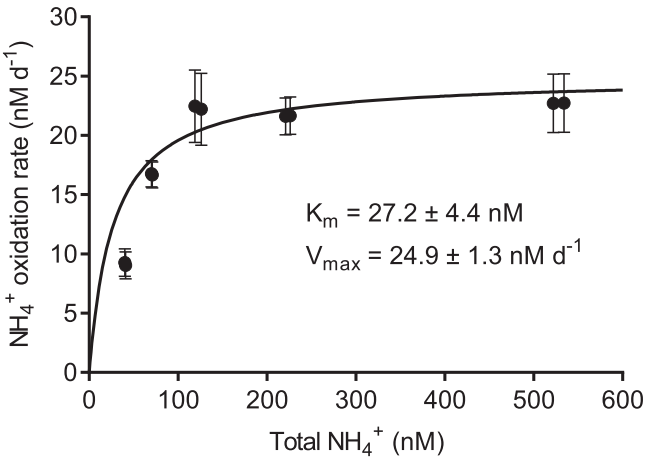

Figure 6. The dependence of NH_4^+ oxidation rate on NH_4^+ concentration at 75 m at offshore station BB1. The rates are plotted against the sum of ambient NH_4^+ and $^{15}NH_4^+$ added. The solid line is fitted based on the Michaelis-Menten equation, where K_m is the half-saturation constant, and V_{max} is the maximum rate of NH_4^+ oxidation. Standard deviations were calculated with Monte Carlo simulation (N = 10000).

fuels oxygen consumption and nitrate reduction. Additionally, horizontal supply of oxygen at the OMZ margin was probably greater than within the OMZ [*Thamdrup et al.*, 2012]. Differences between the coastal OMZs (stations BB2 and 21) and the OMZ margin (stations 10 and 20) can be attributed to the relationship between the amount of organic matter supply and the degree of anoxia/NO_2^- accumulation. These differences include the thickness of the anoxic layer, the maximum concentration of NO_2^- in the SNM and the maximum NH_4^+ concentration, all of which are greater in the coastal OMZ. Nitrification rates also followed this pattern, being generally greater in the coastal than offshore region, probably due to greater amount of organic matter flux in the coastal OMZ.

4.2. NH_4^+ Oxidation and Its Determinants

NH_4^+ oxidation rates displayed subsurface maxima in the oxycline at all stations, and decreased with depth below the maximum (Figures 2c–4c). This pattern directly reflects the magnitude of organic matter flux in the water column, which is the source of NH_4^+ [*Ward and Zafiriou*, 1988]. The NH_4^+ oxidation rates measured in this study could be potential rates, because final NH_4^+ concentration (400–1600 nM) in the incubations often exceeded ambient NH_4^+ levels. The results of the kinetics experiment indicate that NH_4^+ oxidation rates should be saturated at these concentrations. Additionally, incubations were performed in the dark, which may have allowed samples taken from the euphotic zone to recover from photoinhibition, and reduced competition for NH_4^+ with phytoplankton [*Eppley et al.*, 1971]. On the other hand, NH_4^+ regeneration, which was not accounted for in our calculation, would dilute the ^{15}N-labeled NH_4^+ pool, and hence lead to underestimation of NH_4^+ oxidation rates. Both isotope dilution and competition with phytoplankton are probably minimal at this level of NH_4^+ addition. In the following discussion, we take the measured rates at face value and consider the three factors (NH_4^+ concentration, oxygen concentration, and light level) likely to control NH_4^+ oxidation.

NH_4^+ availability is one of the controls of NH_4^+ oxidation rates in our experiments. The classic Michaelis-Menten response of NH_4^+ oxidation rates to NH_4^+ concentration in the kinetics experiment demonstrated that the natural assemblage of ammonia oxidizers had extremely high affinity for NH_4^+ (27.2 ± 4.4 nM, Figure 6). The half-saturation concentration for NH_4^+ of this particular sample, collected from the PNM at the offshore station BB1, was the lowest among all published values determined in both culture and field studies. The half-saturation concentration for NH_4^+ of *Nitrosopumilus maritimus* determined in culture was 133 nM [*Martens-Habbena et al.*, 2009]. The half-saturation concentration for NH_4^+ for the natural assemblage was 65 ± 41 nM at the PNM in the Sargasso Sea [*Newell et al.*, 2013], and 98 ± 14 nM below the euphotic part of the water column of Hood Canal, Puget Sound, WA, USA [*Horak et al.*, 2013]. The Sargasso Sea at least is as oligotrophic as the ETSP offshore OMZ, and the K_m's for NH_4^+ by the natural assemblages of ammonia oxidizers in these two regions were not significantly different. *N. maritimus* was isolated from a nutrient-rich environment and its K_m is higher than all of the reported natural assemblages but still in the nM range. The very low K_m for NH_4^+ by the natural assemblages of ammonia oxidizers in the ETSP indicates that they have adapted to the oligotrophic environment and are strong competitors for NH_4^+.

On the other hand, the linear relationship between NH_4^+ oxidation rates and *in situ* NH_4^+ concentrations measured in the upper oxycline at all stations (Figure 7a) reflects the population size of ammonia oxidizers. This is because all incubations in these experiments were performed at NH_4^+ concentrations (400–1600 nM) above saturation NH_4^+ concentrations (Figure 6), and therefore measured the potential of NH_4^+ oxidation.

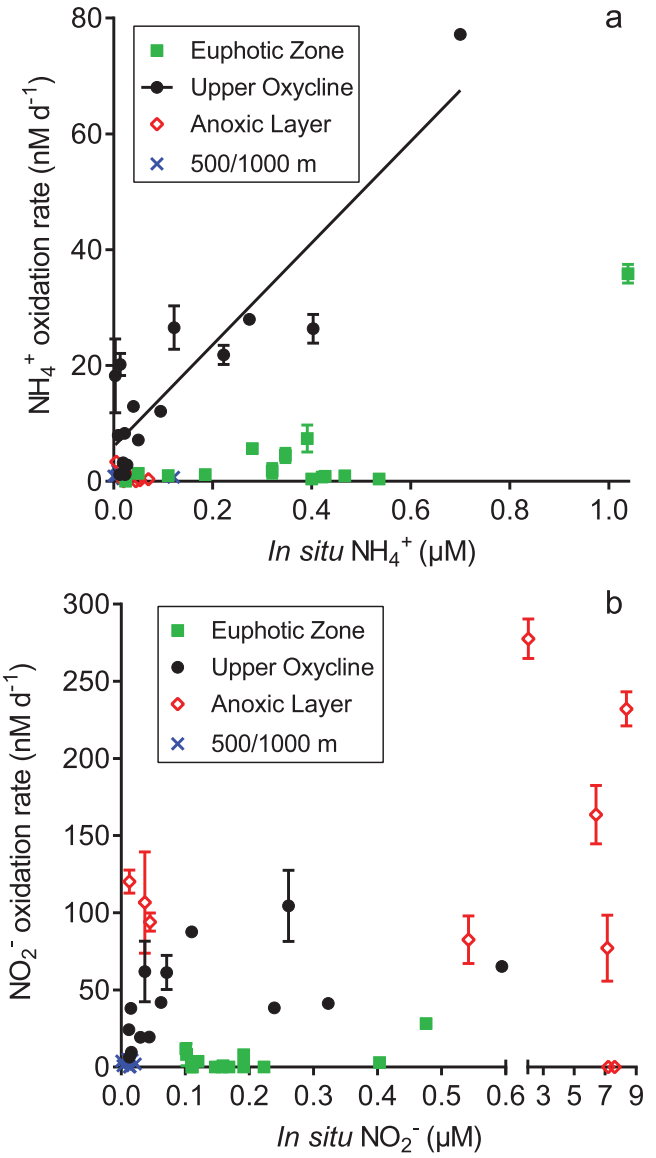

Figure 7. The relationship between (a) NH_4^+ oxidation rates and *in situ* NH_4^+ concentration, and (b) NO_2^- oxidation rates and *in situ* NO_2^- concentration. A linear regression was performed for NH_4^+ oxidation rates from the upper oxycline ($p < 0.0001$, $R^2 = 0.82$).

Previous studies have also found a linear relationship between NH_4^+ oxidation rates and *in situ* NH_4^+ concentrations. During a strong upwelling event in the Washington coastal waters, NH_4^+ oxidation rates increased with *in situ* NH_4^+ concentrations, and did not saturate at NH_4^+ concentrations as high as 3 μM [*Ward*, 1985]. Similarly, in the California coastal waters which are also under the influence of upwelling, nitrification rates displayed a linear correlation with *in situ* NH_4^+ concentrations up to 0.9 μM [*Smith et al.*, 2014b].

Indeed, the population size of ammonia oxidizers, measured as the archaeal *amoA* gene abundance, showed a robust positive linear correlation with NH_4^+ oxidation rates in the upper oxycline (Figure 10). This indicates that when no other environmental variables are limiting ammonia-oxidizing assemblages, their population size would directly respond to NH_4^+ availability, which is indicated by NH_4^+ concentrations. Such a linear correlation has also been identified in previous studies. In the Gulf of California, both the archaeal *amoA* gene abundance of Water Column Group A and marine Crenarchaeota 16S rRNA gene copies were positively correlated with NH_4^+ oxidation rates [*Beman et al.*, 2008]. Similarly, nitrification rates were found to be positively correlated with the archaeal *amoA* gene abundance of Water Column Group A in the surface waters off the California coast [*Smith et al.*, 2014a].

Ammonia oxidizers responded to higher NH_4^+ availability not only at the population level, but also at the cellular level. The average per cell NH_4^+ oxidation rate in this study (0.81 fmol $cell^{-1}$ d^{-1}), as revealed by the slope of the linear regression line in Figure 10, was 7 times lower than that reported from the California coastal water (6.48 fmol $cell^{-1}$ d^{-1}) [*Smith et al.*, 2014a], where the NH_4^+ supply was higher than in the ETSP. We also calculated per cell NH_4^+ oxidation rates for each individual sample for which both NH_4^+ oxidation rates and *amoA* gene abundance data were available. Per cell NH_4^+ oxidation rate ranged from 0.1 to 2.1 fmol $cell^{-1}$ d^{-1}, and was similar to rates measured in other field experiments (0.2–15 fmol $cell^{-1}$ d^{-1} in *Santoro et al.* [2010], 0.10–5.96 fmol $cell^{-1}$ d^{-1} in *Urakawa et al.* [2014], 0.1–4.1 fmol $cell^{-1}$ d^{-1} in *Peng et al.* [2015]), but on the lower range of those determined in culture (1.8–15.4 fmol $cell^{-1}$ d^{-1} in *Konneke et al.* [2005]; 2–4 fmol $cell^{-1}$ d^{-1} in *Wuchter et al.* [2006]).

The control of NH_4^+ availability on NH_4^+ oxidation rates is not only manifested on large spatial scales and molecular levels, but also reflected on temporal scales such as seasonal cycles. The NH_4^+ supply for nitrification in the ETSP originates from remineralization of organic matter produced in the euphotic zone.

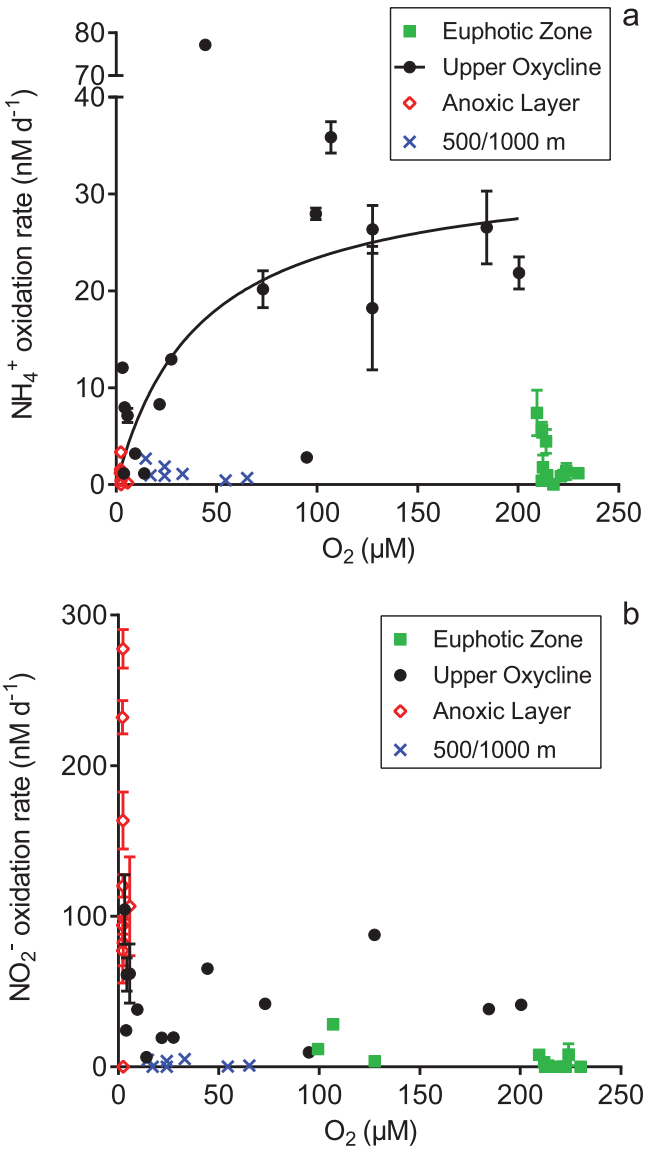

Figure 8. The relationship between oxygen concentration and (a) NH_4^+ oxidation rates, and (b) NO_2^- oxidation rates. The solid line is fitted based on the Michaelis-Menten equation, with a half-saturation concentration for O_2 of 34.8 ± 2.5 μM (Monte Carlo simulation N = 10000).

Upwelling is one of the primary physical processes that transport nutrients to the euphotic zone and hence fuels primary production. As a result, primary productivity in the ETSP also displays a seasonal cycle [*Berelson et al.*, 2015; *Pennington et al.*, 2006]. NH_4^+ oxidation rates measured in this study fell into the low range of NH_4^+ oxidation rates reported from the ETSP OMZ previously (Table 2). This could be a result of the sampling time of austral winter (July 2013), when the productivity is relatively low [*Berelson et al.*, 2015].

Besides NH_4^+, oxygen is also a critical control on the rates of NH_4^+ oxidation. Per cell NH_4^+ oxidation rates from the upper oxycline of stations BB1 and BB2 showed a Michaelis-Menten relationship with oxygen concentration (Figure 9) with a half-saturation concentration (K_m) of 2.0 ± 1.2 μM, which is very close to the K_m determined with *Nitrosopumilus maritimus* (3.9 ± 0.6 μM) [*Martens-Habbena et al.*, 2009]. This indicates that the oxygen level directly controls NH_4^+ oxidation rates on a molecular level. The oxygen concentration measurements used to calculate the K_m were from the SBE oxygen sensor, which had a detection limit of 2.0 μM. Hence the actual K_m for oxygen is likely even lower than 2.0 μM. In fact, a very low K_m for oxygen (0.33 ± 0.13 μM) has been measured by *Bristow et al.* [2013] in the ETSP, suggesting the ammonia-oxidizing assemblage in OMZs is adapted to extremely low oxygen concentrations. Such high affinity for oxygen by ammonia oxidizers implies that their activity is only affected by a narrow range of oxygen concentration, which is found at the oxic-anoxic interface of OMZs. At oxygen concentrations > 2 μM in the upper oxycline, oxygen is unlikely to limit NH_4^+ oxidation rates. Therefore, the Michealis-Menten-like relationship between NH_4^+ oxidation rates and *in situ* oxygen concentration in the upper oxycline (Figure 8a) probably does not reflect NH_4^+ oxidation rates controlled by oxygen concentrations, but rather by the NH_4^+ availability, which covaried with oxygen.

The relationships between NH_4^+ oxidation rates and *in situ* NH_4^+ and oxygen concentrations also reveal that when neither substrate is limiting, light could inhibit NH_4^+ oxidation (Figures 7 and 8). NH_4^+ oxidation rates were slower in the euphotic zone than in the upper oxycline at the same NH_4^+ concentrations (Figure 7a), suggesting that light controls the population size, and therefore potential oxidation rates, in the euphotic zone even when samples are incubated in the dark. Light inhibits nitrifying activities by damaging the cytochromes in bacterial ammonia and nitrite oxidizers [*Ward*, 2011] but the mechanisms for light inhibition of AOA is unknown. These experiments demonstrated that photoinhibition of nitrification is not complete at 10%

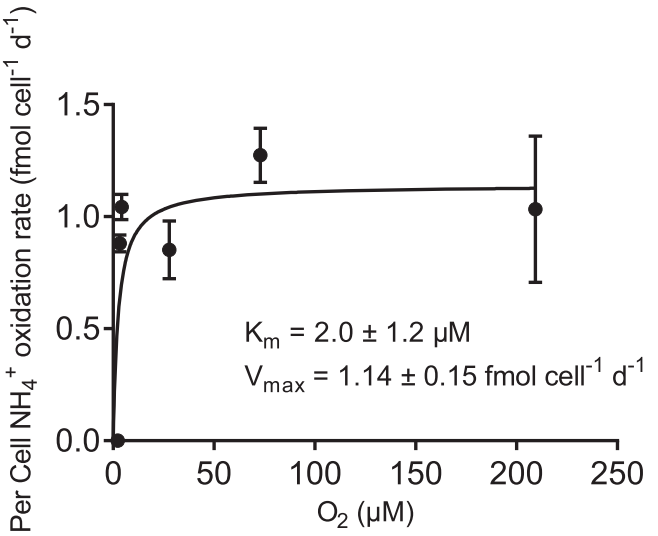

Figure 9. The relationship between NH_4^+ oxidation rates normalized by *amoA* gene abundances and oxygen concentration. The samples were from the upper oxycline at stations BB1 and BB2. The solid line is fitted based on the Michaelis-Menten equation, with a half-saturation concentration for O_2 of 2.7 ± 0.8 μM (Monte Carlo simulation N = 10000).

surface irradiance. The partial inhibition of NH_4^+ oxidation by light is consistent with a number of previous studies both in the field and in culture. *Horrigan et al.* [1981] found that ammonia oxidizers from sea surface films were partially inhibited under the 8:16 light-dark cycle at a light level (167 μE m^{-2} s^{-1}) very similar to that in our incubations (167 μE m^{-2} s^{-1} at station BB1 and 127 μE m^{-2} s^{-1} at station BB2, supporting information Figure S2). Culture studies of AOA and AOB both demonstrated that photoinhibition of nitrifying activity is only partial, and the degree of inhibition varies among species [*Guerrero and Jones*, 1996; *Merbt et al.*, 2012; *Qin et al.*, 2014]. Moreover, there is evidence suggesting that nitrification activity in the euphotic zone was inhibited during the day, but could recover at night [*Horrigan et al.*, 1981; *Qin et al.*, 2014].

A confounding factor to photoinhibition of nitrification in the euphotic zone is the competition between ammonia oxidizers and phytoplankton for NH_4^+. Because all of our incubations were performed in the dark, such competition for NH_4^+ is likely minimized. NH_4^+ uptake by phytoplankton has been shown to control nitrification in the euphotic zone of California coastal waters, where light did not have an inhibitory effect on nitrification [*Smith et al.*, 2014b].

The lack of response of NH_4^+ oxidation to the addition of Fe_2O_3 and MnO_2 at the SNM suggests that the ammonia-oxidizing microorganisms are incapable of oxidizing NH_4^+ using metals as oxidants in place of oxygen. It is worth noting though, that at the deep chlorophyll maximum (DCM) at station BB2, the NH_4^+ oxidation rate was eight-fold higher with the addition of 9.6 μM of oxygen (Figure 5). Given their low K_m for oxygen, these ammonia oxidizers should have reached the maximum NH_4^+ oxidation rate per cell. This suggests that the large population of AOA at the oxic-anoxic interface are metabolically ready for oxygen supply, either from diffusion/turbulent mixing from the upper oxycline, or from the oxygen production by the *Prochlorococcus* at the DCM. The same addition of oxygen to the SNM samples had no effect, suggesting that the AOA detected in the anoxic layer are not metabolically active with respect to aerobic pathways even when oxygen is supplied.

4.3. NH_4^+ Oxidation and N_2O Production

The proximity of the subsurface maxima of NH_4^+ oxidation rates and N_2O concentration implies that NH_4^+ oxidation is likely a major pathway of N_2O production in the upper oxycline. *Farias et al.* [2009] have attributed the N_2O production in the upper oxycline of the ETSP to both NH_4^+ oxidation and partial denitrification (the reduction of NO_2^-/NO_3^- to N_2O). However, it is worth noting that bacterial ammonia oxidizers can also produce N_2O through denitrification [*Casciotti and Ward*, 2001]. The pathway by which N_2O is produced by AOA is still not clear. Nitrification (i.e., from added $^{15}NH_4^+$) was the only pathway of N_2O production at oxygen concentrations above 5 μM in the upper oxycline detected by ^{15}N tracer experiments on the same cruise [*Ji et al.*, 2015]. This result indicates that nitrification is responsible for the N_2O concentration maxima in the upper oxycline, which were found at oxygen concentration of 93.2 μM at station BB1 and 27.9 μM at station BB2. Importantly, the upper oxycline is the depth interval from which N_2O might be emitted to the atmosphere by mixing of surface waters.

4.4. NO_2^- Oxidation Rates

NO_2^- oxidation rates also displayed a subsurface maximum in the upper oxycline, but in the anoxic layer, high rates of NO_2^- oxidation were measured. The subsurface maximum of NO_2^- oxidation was deeper than that of NH_4^+

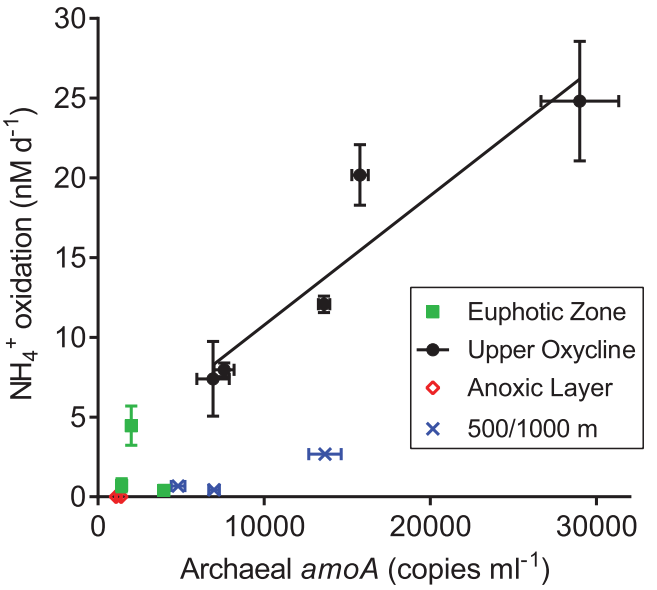

Figure 10. The relationship between archaeal *amoA* gene abundance and NH_4^+ oxidation rates at stations BB1 and BB2. The slope of the linear regression for data from the upper oxycline is 0.00081, with an R^2 of 0.88 ($p = 0.018$).

oxidation. Some of the NO_2^- oxidation rates measured in this study were likely potential rates for the same reasons mentioned earlier for NH_4^+ oxidation rates. Although the NO_2^- oxidation rate did not show a clear response to the total NO_2^- concentration (supporting information Figure S3), it is clear that the NO_2^- oxidation rate has saturated at NO_2^- concentrations greater than 3.2 μM. Hence at the SNM, where NO_2^- concentrations were high, the measured NO_2^- oxidation rates were not affected by substrate addition. The NO_2^- oxidation rates measured in this study are comparable to previous reports from OMZs (Table 2).

The decrease of NO_2^- oxidation rates with depth below 75 m, excluding the samples from the anoxic layer (supporting information Figure S4), suggests that NO_2^- oxidation in the upper oxycline also depends on remineralization for substrate supply. The linear relationship between NO_2^- oxidation rates and NO_2^- concentration at < 0.1 μM in the upper oxycline indicates that the substrate dependence of NO_2^- oxidation is the strongest at low NO_2^- concentrations (Figure 7b). Because NO_2^- oxidation rates were generally higher than NH_4^+ oxidation rates, there was likely another source of NO_2^-. Previous studies in the ETSP showed that NO_3^- reduction is another major source of NO_2^- in the upper oxycline [*Kalvelage et al.*, 2013; *Lipschultz et al.*, 1990]. The rate of NO_3^- reduction to NO_2^- was generally higher at lower oxygen levels in the upper oxycline of the ETSP, and potentially supporting a large population of nitrite oxidizers at those depths. This might be one of the reasons for the observed deeper subsurface maximum of NO_2^- oxidation rates than that of NH_4^+ oxidation.

Recent studies have found a Michaelis-Menten relationship between NO_2^- oxidation rates and oxygen concentration in the *in situ* NO_2^--oxidizing assemblage in both the Namibian and the ETSP OMZs [*Bristow et al.*, 2013; *Fussel et al.*, 2012]. The half-saturation concentration for oxygen (K_m) determined using incubations with $^{15}NO_2^-$ and manipulation of the oxygen level with additions of oxygen-saturated seawater was very low ($K_m = 0.78$ μM in the ETSP and ~4 μM in the Namibian OMZ). However, there was no clear relationship between

Table 2. A Summary of NH_4^+ and NO_2^- Oxidation Rates Measured in the Major Oceanic OMZs Using ^{15}N Technique[a]

OMZ Region	Max/Median of Max NH_4^+ Oxidation (nM d^{-1})	Max/Median of Max NO_2^- Oxidation (nM d^{-1})	Method	Sampling Date	Reference
ETSP	77/22	278/107	^{15}N	Jun/Jul 2013	This study
	288/85	605/202	^{15}N	Feb/Mar 1985	*Lipschultz et al.* [1990]
	4900/144	N.M.	^{15}N	Apr 2005	*Lam et al.*] 2009]
	89/33	186/37	^{15}N	Dec 2008 to Feb 2009	*Kalvelage et al.* [2013]
ETNP	46/38	115/81	^{15}N	Nov 1982/ May 1983	*Ward* [1987]
	22/12	N.M.	^{15}N	Nov 1983	*Ward and Zafiriou* [1988]
	23/15	N.M.	^{15}N	May/Jun 2000	*Sutka et al.* [2004]
	348/47	136/57	^{15}N	Jul/Aug 2008	*Beman et al.* [2013]
	36/28	536/312	^{15}N	Mar/Apr 2012	*Peng et al.* [2015]
Arabian Sea	21/9	N.M.	^{15}N	Sep/Oct 2007	*Newell et al.* [2011]
	4/4	N.M.	^{15}N	Sep/Oct 2007	*Lam et al.* [2011]

[a]Max: the maximum NH_4^+ andNO_2^- rates found in each study. Median of Max: the median of maximum NH_4^+ and NO_2^- rates measured at each sampling station within the study. N.M.: not measured.

NO_2^- oxidation rates and *in situ* oxygen concentration in the Namibian OMZ [*Fussel et al.*, 2012]. Our incubation measurements did not reveal any clear relationship between NO_2^- oxidation rates and *in situ* oxygen concentration across several stations (Figure 8b). This may be due to the different population size of NO_2^--oxidizers in each sample. Nitrite oxidizers were not enumerated in this study because we have not optimized a qPCR protocol for an appropriate functional gene and the nitrite oxidizers are too diverse to allow quantification by one set of 16S rRNA primers [*Daims et al.*, 2011]. High rates of NO_2^- oxidation measured in the anoxic layer in the absence of molecular oxygen were also reported previously [*Kalvelage et al.*, 2013; *Lipschultz et al.*, 1990; *Peng et al.*, 2015]. However, no alternative electron acceptors have been identified and these high rates remain unexplained. The physiology and biochemical potential of nitrite oxidizers is not well known and investigation of their anaerobic metabolism may yet provide some explanation for high anoxic oxidation rates.

NO_2^- oxidation appeared to be more sensitive to light than NH_4^+ oxidation, because NO_2^- oxidation was detected in only 6 out of the 12 samples collected from the euphotic zone in which NH_4^+ oxidation was detected. This is consistent with a culture study comparing the photoinhibition by AOB and NOB [*Guerrero and Jones*, 1996]. On the other hand, when NO_2^- oxidation was not completely inhibited in the euphotic zone, it might also be colimited by NO_2^- supply, because NH_4^+ oxidation rates in the euphotic zone were either very low or below detection. NO_2^- oxidation rates measured in the light/dark experiment were too variable to be significantly different than zero (Table 1).

5. Conclusion

The NH_4^+ oxidation rates in the ETSP mainly displayed a depth distribution consistent with ultimate control by the vertical flux of organic material, i.e., NH_4^+ supply. In addition, NH_4^+ oxidation rates depended on NH_4^+ concentration, oxygen concentration, and light. In the euphotic zone, NH_4^+ oxidation was partially photoinhibited, and in the anoxic layer and the oxic-anoxic interface of OMZs, NH_4^+ oxidation was limited by oxygen concentration. NH_4^+ oxidation displayed extremely high affinity for both NH_4^+ and oxygen. The positive linear correlations between NH_4^+ oxidation rates and *in situ* NH_4^+ concentrations and *amoA* gene abundances in the upper oxycline indicate that natural assemblage of ammonia oxidizers responds to *in situ* NH_4^+ concentrations by adjusting their population size, which determines the NH_4^+ oxidation potential. The depth distribution of archaeal and bacterial *amoA* gene abundances and N_2O concentration suggests that AOA were predominantly responsible for NH_4^+ oxidation, which was the primary source of N_2O production in the upper oxycline of the OMZ.

Besides the primary influence from the vertical organic matter flux, NO_2^- oxidation was also controlled by substrate availability and light. The depth of the subsurface NO_2^- oxidation maximum in the upper oxycline was greater than that of NH_4^+ oxidation maximum. At this depth, the NO_2^- oxidation rates were higher than NH_4^+ oxidation rates, suggesting an additional source of NO_2^- in the lower part of the upper oxycline near the oxic-anoxic interface. Considerable rates of NO_3^- reduction to NO_2^- at this depth have been measured in the ETSP previously [*Kalvelage et al.*, 2013; *Lipschultz et al.*, 1990], and might be a major source of NO_2^- for NO_2^- oxidation. The high NO_2^- oxidation in the absence of molecular oxygen in the anoxic layer of OMZs remains unexplained.

Acknowledgments

This work was supported by National Science Foundation Oceanography (OCE) awards 10-29951 to B.B.W. and A.J. and NSF (OCE) award to A.H.D. 10-29316. We are indebted to Calvin Mordy for measuring nutrients, Niels Peter Revsbech for the STOX sensor data, the crew of the R/V Thomas Thompson for general assistance, to Karen Casciotti for providing the NO_2^- stable isotope standard, to Daniel Sigman for consultation, and Sergey Oleynik for superb technical assistance in the laboratory. The data used in this paper will be deposited on http://www.princeton.edu/nitrogen.

References

Beman, J. M., B. N. Popp, and C. A. Francis (2008), Molecular and biogeochemical evidence for ammonia oxidation by marine Crenarchaeota in the Gulf of California, *ISME J.*, *2*(4), 429–441, doi:10.1038/ismej.2007.118.

Beman, J. M., B. N. Popp, and S. E. Alford (2012), Quantification of ammonia oxidation rates and ammonia-oxidizing archaea and bacteria at high resolution in the Gulf of California and eastern tropical North Pacific Ocean, *Limnol. Oceanogr. Methods*, *57*(3), 711–726, doi:10.4319/lo.2012.57.3.0711.

Beman, J. M., J. Leilei Shih, and B. N. Popp (2013), Nitrite oxidation in the upper water column and oxygen minimum zone of the eastern tropical North Pacific Ocean, *ISME J.*, *7*(11), 2192–2205, doi:10.1038/ismej.2013.96.

Berelson, W. M., W. Z. Haskell, M. Prokopenko, A. N. Knapp, D. E. Hammond, N. Rollins, and D. G. Capone (2015), Biogenic particle flux and benthic remineralization in the Eastern Tropical South Pacific, *Deep Sea Res., Part I*, *99*, 23–34, doi:10.1016/j.dsr.2014.12.006.

Bristow, L. A., T. Dalsgaard, L. Tiano, D. B. Mills, O. Ulloa, D. Canfield, N. P. Revsbech, and B. Thamdrup (2013), High sensitivity of ammonia and nitrite oxidation rates to namomolar oxygen concentrations, *Mineral. Mag.*, *77*(5), 775, doi:10.1180/minmag.2013.077.5.2.

Bullister, J. L., and D. P. Wisegarver (2008), The shipboard analysis of trace levels of sulfur hexafluoride, chlorofluorocarbon-11 and chlorofluorocarbon-12 in seawater, *Deep Sea Res., Part I*, *55*(8), 1063–1074, doi:10.1016/j.dsr.2008.03.014.

Casciotti, K. L., and B. B. Ward (2001), Dissimilatory nitrite reductase genes from autotrophic ammonia-oxidizing bacteria, *Appl. Environ. Microbiol.*, *67*(5), 2213–2221, doi:10.1128/AEM.67.5.2213-2221.2001.

Casciotti, K. L., C. Buchwald, and M. McIlvin (2013), Implications of nitrate and nitrite isotopic measurements for the mechanisms of nitrogen cycling in the Peru oxygen deficient zone, *Deep Sea Res., Part I*, *80*, 78–93, doi:10.1016/j.dsr.2013.05.017.

Codispoti, L. A., J. A. Brandes, J. P. Christensen, A. H. Devol, S. W. A. Naqvi, H. W. Paerl, and T. Yoshinari (2001), The oceanic fixed nitrogen and nitrous oxide budgets: Moving targets as we enter the anthropocene?, *Sci. Mar.*, *65*, 85–105.

Daims, H., S. Lucker, D. Le Paslier, and M. Wagner (2011), Diversity, environmental genomics, and ecophysiology of nitrite-oxidizing bacteria, *Nitrification*, 295–322, doi:10.1128/9781555817145.ch12.

DeVries, T., C. Deutsch, F. Primeau, B. Chang, and A. Devol (2012), Global rates of water-column denitrification derived from nitrogen gas measurements, *Nat. Geosci.*, *5*(8), 547–550, doi:10.1038/NGEO1515.

Dore, J. E., T. Houlihan, D. V. Hebel, G. Tien, L. Tupas, and D. M. Karl (1996), Freezing as a method of sample preservation for the analysis of dissolved inorganic nutrients in seawater, *Mar. Chem.*, *53*(3-4), 173–185, doi:10.1016/0304-4203(96)00004-7.

Eppley, R. W., J. N. Rogers, J. J. Mccarthy, and A. Sournia (1971), Light/dark periodicity in nitrogen assimilation of marine phytoplankters Skeletonema-Costatum and Coccolithus-Huxleyi in N-limited chemostat culture, *J. Phycol.*, *7*(2), 150, doi:10.1111/j.0022-3646.1971.00150.x.

Farias, L., M. Castro-Gonzalez, M. Cornejo, J. Charpentier, J. Faundez, N. Boontanon, and N. Yoshida (2009), Denitrification and nitrous oxide cycling within the upper oxycline of the eastern tropical South Pacific oxygen minimum zone, *Limnol. Oceanogr. Methods*, *54*(1), 132–144, doi:10.4319/lo.2009.54.1.0132.

Francis, C. A., K. J. Roberts, J. M. Beman, A. E. Santoro, and B. B. Oakley (2005), Ubiquity and diversity of ammonia-oxidizing archaea in water columns and sediments of the ocean, *Proc. Natl. Acad. Sci. U. S. A.*, *102*(41), 14,683–14,688, doi:10.1073/pnas.0506625102.

Fussel, J., P. Lam, G. Lavik, M. M. Jensen, M. Holtappels, M. Gunter, and M. M. Kuypers (2012), Nitrite oxidation in the Namibian oxygen minimum zone, *ISME J.*, *6*(6), 1200–1209, doi:10.1038/ismej.2011.178.

Granger, J., and D. M. Sigman (2009), Removal of nitrite with sulfamic acid for nitrate N and O isotope analysis with the denitrifier method, *Rapid Commun. Mass Spectrom.*, *23*(23), 3753–3762, doi:10.1002/rcm.4307.

Guerrero, M. A., and R. D. Jones (1996), Photoinhibition of marine nitrifying bacteria .1. Wavelength-dependent response, *Mar. Ecol. Prog. Ser.*, *141*(1-3), 183–192, doi:10.3354/Meps141183.

Horak, R. E., W. Qin, A. J. Schauer, E. V. Armbrust, A. E. Ingalls, J. W. Moffett, D. A. Stahl, and A. H. Devol (2013), Ammonia oxidation kinetics and temperature sensitivity of a natural marine community dominated by Archaea, *ISME J.*, *7*(10), 2023–2033, doi:10.1038/ismej.2013.75.

Horrigan, S. G., A. F. Carlucci, and P. M. Williams (1981), Light inhibition of nitrification in sea-surface films, *J. Mar. Res.*, *39*(3), 557–565.

Ji, Q., A. R. Babbin, A. Jayakumar, S. Oleynik, and B. B. Ward (2015), Nitrous oxide production by nitrification and denitrification in the Eastern Tropical South Pacific oxygen minimum zone, *Geophys. Res. Lett.*, *42*, 10,755–10,764, doi:10.1002/2015GL066853.

Kalvelage, T., G. Lavik, P. Lam, S. Contreras, L. Arteaga, C. R. Löscher, A. Oschlies, A. Paulmier, L. Stramma, and M. M. M. Kuypers (2013), Nitrogen cycling driven by organic matter export in the South Pacific oxygen minimum zone, *Nat. Geosci.*, *6*(3), 228–234, doi:10.1038/ngeo1739.

Konneke, M., A. E. Bernhard, J. R. de la Torre, C. B. Walker, J. B. Waterbury, and D. A. Stahl (2005), Isolation of an autotrophic ammonia-oxidizing marine archaeon, *Nature*, *437*(7058), 543–546, doi:10.1038/nature03911.

Lam, P., G. Lavik, M. M. Jensen, J. van de Vossenberg, M. Schmid, D. Woebken, D. Gutierrez, R. Amann, M. S. Jetten, and M. M. Kuypers (2009), Revising the nitrogen cycle in the Peruvian oxygen minimum zone, *Proc. Natl. Acad. Sci. U. S. A.*, *106*(12), 4752–4757, doi:10.1073/pnas.0812444106.

Lam, P., M. M. Jensen, A. Kock, K. A. Lettmann, Y. Plancherel, G. Lavik, H. W. Bang, and M. M. Kuypers (2011), Origin and fate of the secondary nitrite maximum in the Arabian Sea, *Biogeosci.*, *8*, 1565–1577, doi:10.5194/bg-8-1565-2011.

Lipschultz, F., S. C. Wofsy, B. B. Ward, L. A. Codispoti, G. Friedrich, and J. W. Elkins (1990), Bacterial transformations of inorganic nitrogen in the oxygen-deficient waters of the eastern tropical South-Pacific Ocean, *Deep Sea Res, Part A*, *37*(10), 1513–1541, doi:10.1016/0198-0149(90)90060-9.

Martens-Habbena, W., P. M. Berube, H. Urakawa, J. R. de la Torre, and D. A. Stahl (2009), Ammonia oxidation kinetics determine niche separation of nitrifying Archaea and Bacteria, *Nature*, *461*(7266), 976–979, doi:10.1038/nature08465.

McIlvin, M. R., and M. A. Altabet (2005), Chemical conversion of nitrate and nitrite to nitrous oxide for nitrogen and oxygen isotopic analysis in freshwater and seawater, *Anal. Chem.*, *77*(17), 5589–5595, doi:10.1021/ac050528s.

McIlvin, M. R., and K. L. Casciotti (2011), Technical updates to the bacterial method for nitrate isotopic analyses, *Anal. Chem.*, *83*(5), 1850–1856, doi:10.1021/ac1028984.

Merbt, S. N., D. A. Stahl, E. O. Casamayor, E. Marti, G. W. Nicol, and J. I. Prosser (2012), Differential photoinhibition of bacterial and archaeal ammonia oxidation, *FEMS Microbiol. Lett.*, *327*(1), 41–46, doi:10.1111/j.1574-6968.2011.02457.x.

Newell, S. E., A. R. Babbin, A. Jayakumar, and B. B. Ward (2011), Ammonia oxidation rates and nitrification in the Arabian Sea, *Global Biogeochem. Cycles*, *25*, GB4016, doi:10.1029/2010GB003940.

Newell, S. E., S. E. Fawcett, and B. B. Ward (2013), Depth distribution of ammonia oxidation rates and ammonia-oxidizer community composition in the Sargasso Sea, *Limnol. Oceanogr. Methods*, *58*(4), 1491–1500, doi:10.4319/lo.2013.58.4.1491.

Peng, X., C. A. Fuchsman, A. Jayakumar, S. Oleynik, W. Martens-Habbena, A. H. Devol, and B. B. Ward (2015), Ammonia and nitrite oxidation in the Eastern Tropical North Pacific, *Global Biogeochem. Cycles*, *29*, 2034–2049, doi:10.1002/2015GB005278.

Peng, X. F., A. Jayakumar, and B. B. Ward (2013), Community composition of ammonia-oxidizing archaea from surface and anoxic depths of oceanic oxygen minimum zones, *Frontiers Microbiol.*, *4*, 177, doi:10.3389/fmicb.2013.00177.

Pennington, J. T., K. L. Mahoney, V. S. Kuwahara, D. D. Kolber, R. Calienes, and F. P. Chavez (2006), Primary production in the eastern tropical Pacific: A review, *Prog. Oceanogr.*, *69*(2-4), 285–317, doi:10.1016/j.pocean.2006.03.012.

Qin, W., S. A. Amin, W. Martens-Habbena, C. B. Walker, H. Urakawa, A. H. Devol, A. E. Ingalls, J. W. Moffett, E. V. Armbrust, and D. A. Stahl (2014), Marine ammonia-oxidizing archaeal isolates display obligate mixotrophy and wide ecotypic variation, *Proc. Natl. Acad. Sci. U. S. A.*, *111*(34), 12,504–12,509, doi:10.1073/pnas.1324115111.

Revsbech, N. P., L. H. Larsen, J. Gundersen, T. Dalsgaard, O. Ulloa, and B. Thamdrup (2009), Determination of ultra-low oxygen concentrations in oxygen minimum zones by the STOX sensor, *Limnol. Oceanogr. Methods*, *7*, 371–381, doi:10.4319/lom.2009.7.371.

Rotthauwe, J. H., K. P. Witzel, and W. Liesack (1997), The ammonia monooxygenase structural gene amoA as a functional marker: Molecular fine-scale analysis of natural ammonia-oxidizing populations, *Appl. Environ. Microbiol.*, *63*(12), 4704–4712.

Santoro, A. E., K. L. Casciotti, and C. A. Francis (2010), Activity, abundance and diversity of nitrifying archaea and bacteria in the central California Current, *Environ. Microbiol.*, *12*(7), 1989–2006, doi:10.1111/j.1462-2920.2010.02205.x.

Santoro, A. E., C. M. Sakamoto, J. M. Smith, J. N. Plant, A. L. Gehman, A. Z. Worden, K. S. Johnson, C. A. Francis, and K. L. Casciotti (2013), Measurements of nitrite production in and around the primary nitrite maximum in the central California Current, *Biogeosciences*, *10*(11), 7395–7410, doi:10.5194/bg-10-7395-2013.

Sigman, D. M., K. L. Casciotti, M. Andreani, C. Barford, M. Galanter, and J. K. Bohlke (2001), A bacterial method for the nitrogen isotopic analysis of nitrate in seawater and freshwater, *Anal. Chem.*, *73*(17), 4145–4153, doi:10.1021/ac010088e.

Smith, J. M., K. L. Casciotti, F. P. Chavez, and C. A. Francis (2014a), Differential contributions of archaeal ammonia oxidizer ecotypes to nitrification in coastal surface waters, *ISME J.*, *8*(8), 1704–1714, doi:10.1038/ismej.2014.11.

Smith, J. M., F. P. Chavez, and C. A. Francis (2014b), Ammonium uptake by phytoplankton regulates nitrification in the sunlit ocean, *PLoS One*, *9*(9), e108173, doi:10.1371/journal.pone.0108173.

Sutka, R. L., N. E. Ostrom, P. H. Ostrom, and M. S. Phanikumar (2004), Stable nitrogen isotope dynamics of ddissolved nitrate in a transect from the North Pacific subtropbical gyre to the eastern tropical North Pacific, *Geochim. Cosmochim. Acta.*, *68*, 517–527, doi:10.1016/S0016-7037(03)00483-6.

Thamdrup, B., T. Dalsgaard, and N. P. Revsbech (2012), Widespread functional anoxia in the oxygen minimum zone of the Eastern South Pacific, *Deep Sea Res., Part I*, *65*, 36–45, doi:10.1016/j.dsr.2012.03.001.

United Nations Educational, Scientific and Cultural Organization (UNESCO) (1994), Protocols for the Joint Global Ocean Flux Study (JGOFS) Core Measurements, vol. 29, UNESCO, N.Y.

Urakawa, H., W. Martens-Habbena, C. Huguet, J. R. de la Torre, A. E. Ingalls, A. H. Devol, and D. A. Stahl (2014), Ammonia availability shapes the seasonal distribution and activity of archaeal and bacterial ammonia oxidizers in the Puget Sound Estuary, *Limnol. Oceanogr. Methods*, *59*(4), 1321–1335, doi:10.4319/lo.2014.59.4.1321.

Ward, B. B. (1985), Light and substrate concentration relationships with marine ammonium assimilation and oxidation rates, *Mar. Chem.*, *16*(4), 301–316, doi:10.1016/0304-4203(85)90052-0.

Ward, B. B. (1987), Nitrogen transformations in the Southern California Bight, *Deep Sea Res., Part A*, *34*, 785–805, doi:10.1016/0198-0149(87)90037-9.

Ward, B. B. (2011), Nitrification in the ocean, *Nitrification*, 325–345, doi:10.1128/9781555817145.ch13.

Ward, B. B., and O. C. Zafiriou (1988), Nitrification and nitric-oxide in the oxygen minimum of the Eastern Tropical North Pacific, *Deep Sea Res., Part A*, *35*(7), 1127–1142, doi:10.1016/0198-0149(88)90005-2.

Ward, B. B., K. A. Kilpatrick, E. H. Renger, and R. W. Eppley (1989), Biological nitrogen cycling in the nitracline, *Limnol. Oceanogr.*, *34*(3), 493–513, doi:10.1016/0198-0149(89)90076-9.

Wuchter, C., et al. (2006), Archaeal nitrification in the ocean, *Proc. Natl. Acad. Sci. U. S. A.*, *103*(33), 12,317–12,322, doi:10.1073/pnas.0600756103.